Preprints of the 21st IFAC World Congress (Virtual)
Berlin, Germany, July 12-17, 2020

# A novel force and motion control strategy for robotic chamfering of gears*

**Jie Hu, Prabhakar R. Pagilla**

*Texas A&M University, College Station, TX 77840 USA (e-mail: j_hu, ppagilla@tamu.edu).*

**Abstract:** Accurate positioning of the workpiece in the robotic work cell is currently required to perform machining operations such as chamfering in order to obtain high quality products. However, registration and workpiece fixturing errors are inevitable and lead to uncertainty in the desired robot end-effector trajectory which will lead to poor quality of the finished product. This paper proposes a method for robotic gear chamfering that can compensate for the registration error of the workpiece while avoiding use of expensive and time-consuming metrology devices for accurately registering the gear in the robot workspace. We highlight the problems in chamfering with workpiece uncertainty when traditional contour following methods are employed. A novel chamfering trajectory based on a part identification procedure is proposed that can account for the gear registration uncertainty. A force control strategy is employed in identifying the gear center and gear root positions. Based on this identification, we employ a novel force/motion strategy that can simultaneously chamfer two edges of the adjacent gear teeth. We have conducted a number of real-time experiments with a six degree-of-freedom robot to evaluate the proposed strategy, and representative chamfering experimental results are presented and discussed.

*Keywords:* Robot manipulators, manufacturing systems, chamfering, motion control, force control

## 1. INTRODUCTION

Chamfering is a common operation in manufacturing to remove sharp edges and burrs. In most industrial sectors, it is predominantly a manual operation where the human operators use hand tools to chamfer part edges, such as gears, cast parts, and surfaces. There is a significant need to automate the chamfering process not only to improve quality and performance, but also to remove health hazard to human operators due to particulate/debris and ergonomic conditions. Robotic manipulators have been widely used in many industrial sectors such as manufacturing, automobile, surface finishing, etc. due to their flexibility and low cost, and these technologies could be potential candidates for automating chamfering of gears or other products. However, compared to robotic deburing and surface finishing such as the work in Pagilla and Yu (2001b); Wen et al. (2019); Ziliani et al. (2007); Zhang et al. (2006); Pagilla and Yu (2001a) where the contact between robot and workpiece is usually surface contact, the contact between end-effector and workpiece is line or even point contact in robotic chamfering. Thus, robotic chamfering requires a more accurate trajectory if contact is to be maintained at all times. Additionally, most modern industrial robotic manipulators only give velocity or position control interface to the users and do not provide the ability to control motor torques for executing a trajectory.

When employing robot manipulators for chamfering, one of the commonly adopted methods is to generate a nominal trajectory from the CAD model of the workpiece and apply the position/orientation of the workpiece in the robot workspace. Asakawa et al. (2000) developed an automatic chamfering system using an industrial robot and applied it to chamfering of a hole by using the chamfering path generated from CAD system. The disadvantage of this trajectory generation method is that the generated trajectory needs to be aligned with the actual workpiece contour, otherwise the end-effector will either remove excessive amount of material or cannot make contact with the workpiece at all. Registration is the process of obtaining the position of the workpiece in the specified coordinate frame by using tools from metrology that provide the accurate location/orientation of the workpiece. This process is usually time-consuming and measuring errors are inevitable. Additionally, geometric deviations exist between the nominal CAD models and manufactured parts. Many methods have been proposed to reduce the position inaccuracy of the workpiece with respect to the robot. Indirect methods are used to modify the trajectories generated based on CAD model instead of relying on metrology tools. Pagilla and Yu (2002) designed a mechatronic platform and implemented a switching controller to adapt to the uncertainties in the

⋆ This work was supported in part by Subaward No. ARM-17-01-F-02 from the Advanced Robotics for Manufacturing ("ARM") under Agreement Number W911NF-17-3-0004 sponsored by the Office of the Secretary of Defense. ARM Project Management was provided by Cara Mazzarini. The views and conclusions contained in this document are those of the authors and should not be interpreted as representing the official policies, either expressed or implied, of either ARM or the Office of the Secretary of Defense of the U.S. Government. The U.S. Government is authorized to reproduce and distribute reprints for Government purposes notwithstanding any copyright notation herein.

constraint surface positions in surface following applications. Kuss et al. (2016) used point clouds registration to align the nominal CAD model with the actual workpiece, but the performance of this method largely depends on the accuracy of the vision system and the robustness of the registration algorithms. Song and Song (2013) tried to improve the CAD model based trajectory generation in robotic deburring by registering the nominal trajectory with chosen points on the workpiece that are obtained from "teaching." An alternative way to generate the trajectory was proposed by Zhang et al. (2006), where visual-servoing was employed to generate a path for robotic deburring of aluminum wheels. An impedance based force control strategy for robotic grinding was developed in Kashiwagi et al. (1990).

Another major source of errors is the positioning and geometry of the work cell or fixture on which the workpiece is mounted in the robot workspace. One of the advantages of robotic machining is the ability to work in a dynamic environment. So, flexible trajectory generation process that can adapt to the changes in the work cell structure is needed for accommodating workpieces with multiple geometries. The method proposed in this paper takes advantage of the high repeatability of industrial robot manipulators and generates a trajectory on-line to avoid costly and time-consuming registration of the workpiece beforehand. In this work, the human operator can place the gear at the designated place in the work cell without precise positioning. We describe a procedure to identify the gear root and gear center by applying a force and motion control strategy. Based on this identification, we generate a novel chamfering trajectory that can simultaneously chamfer the edges of two adjacent gear teeth with an abrasive tool that is referred to as the cone stone. The trajectory generated this way can also take into account the position change during gear mounting and avoid registration for each new gear mounted in the work cell.

The rest of this paper is organized as the following. Section 2 proposes the problems in robotic chamfering. Section 3 discusses the proposed identification process of gear center and gear root, and a novel chamfering trajectory. Section 4 discusses the force control in the identification process. Experiment setup and chamfering results are in Section 5. Section 6 is the conclusion and summary.

## 2. PROBLEM DESCRIPTION

Fig. 1 is a simplified illustration of the work cell setup for chamfering of gears using a robot. Notice that the outer edge of the gear denoted as part A in the figure is chamfered before the gear is cut from a single steel stock. Then, what needs to be chamfered after the gear is cut is the rest of the contour denoted as part B. The common approach is to design a trajectory that follows the contour of the gear. An offset can be added to the contour of the gear considering the geometry of the tool tip to achieve desired material removal. Uniform chamfer with the desired angle can be obtained under the assumption that the planned trajectory aligns with the actual gear perfectly or within tolerance. However, in practice, uncertainty of the location/orientation of the workpiece with respect to the robot may always exist. To quantify and

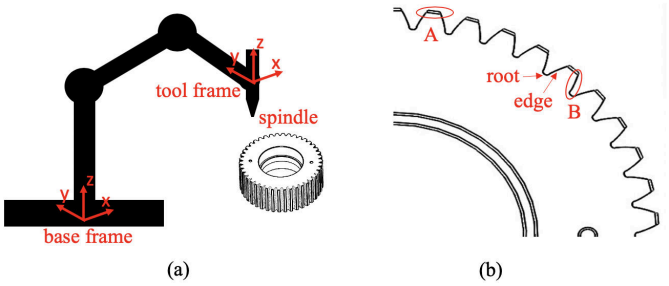


Fig. 1. Robotic chamfering

visualize the possible errors due to setup and registration of the gear for robotic chamfering, assuming the whole trajectory is obtained by rotating one gear tooth contour, an illustration is provided in Fig. 2. Asterisks represent the gear roots while the gear teeth contour is ignored to simplify the representation. The error between the nominal gear root and the actual gear root can be decomposed into two components: one along the radial direction and the other perpendicular to it. Due to this error, the contact between the chamfering tool and the gear will change as the robot chamfers on different gear teeth. Due to error that is perpendicular to radial direction, chamfering tool will make contact with some gear teeth on one single edge while making contact on the other edge with other gear teeth. This is observed in practice and will lead to serious product quality variation.

To calculate the error magnitude, considering Fig. 2(b), the nominal gear center $O$ has error $\Delta$ with respect to the actual gear center $O'$, i.e., $OO' = \Delta$, the nominal point $Q$ is obtained by rotating the start point $P$ around the nominal center $O$ by 90°, and the actual point $Q'$ is obtained by rotating the start point $P$ around the actual center $O'$ by 90°. Assuming that the angle formed between $OO'$ and the $x$ axis is $\theta$. We can derive the following relations:

$$OP = OQ = r \tag{1}$$

$$O'P = O'Q' = R \tag{2}$$

$$R = \sqrt{r^2 + \Delta^2 - 2r\cos(\pi - \theta)\Delta} \tag{3}$$

$$\beta = \arcsin\left(\frac{\Delta \sin(\pi - \theta)}{R}\right) \tag{4}$$

$$D = \sqrt{R^2 + \Delta^2 - 2R\Delta\cos\left(\frac{\pi}{2} - \theta + \beta\right)} \tag{5}$$

$$\gamma^2 = r^2 + D^2 - 2rD\cos\left(\beta + \arcsin\left(\frac{\sin(\frac{\pi}{2} - \theta + \beta)\Delta}{D}\right)\right) \tag{6}$$

To illustrate the impact of the error distribution on chamfer quality, assuming $\Delta = 3$ mm in the above equations, the distance between $Q$ and $Q'$ will be 4.3 mm. Thus, there will be a gap between the tool tip and the gear when the robot is following the trajectory which can cause damage to the tool and the gear.

## 3. PROPOSED CHAMFERING METHOD AND TRAJECTORY DESIGN

This section presents an approach to gear chamfering by using a cone stone type abrasive with a novel trajectory. The shape of the cone stone is shown in Fig. 3. The

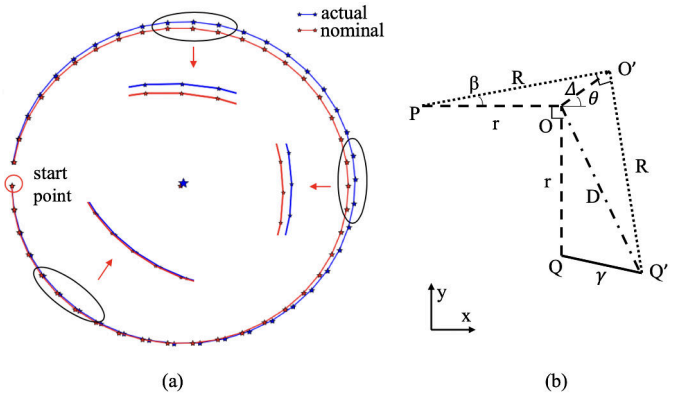


Fig. 2. Trajectory obtained by rotating the first feature (a) Error distribution (b) Error calculation

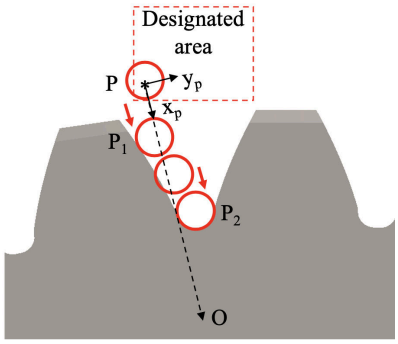


Fig. 3. Identification of the gear root

proposed method provides a solution to compensate for the registration error that causes positioning error of the gear and subsequently chamfering quality problems discussed in the previous section.

There are two important elements in the proposed method: abrasive selection and trajectory design. The motivation for the use of cone stone is twofold. By using the cone stone, both sides of the gear teeth can be chamfered at the same time, as is shown in Fig. 4(a) from position B to C. On the other hand, force control can be adopted to adjust the position of the cone stone such that the cone stone can traverse along the center line of the gear teeth to remove the same amount of the material on both adjacent gear edges. Although force control can also be used with chamfer cutter in contour following theoretically, the implementation when using cone stone is more straightforward since the contour of the gear teeth is an involute and not a straight line. In this case, normal direction of current position needs to be known in order to decouple the motion and force control. And this is not possible without knowing the accurate position of the gear. After the abrasive selection, the chamfering workflow is the following: the center of the gear is identified by contacting the inner diameter of the gear at several points, the end-effector traverses to the designated area to start gear root identification using the proposed force motion control strategy and followed by gear chamfering.

Robot end-effector mounted with probe starts at the approximate gear center and is commanded to move along a random vector at specified velocity until the probe makes

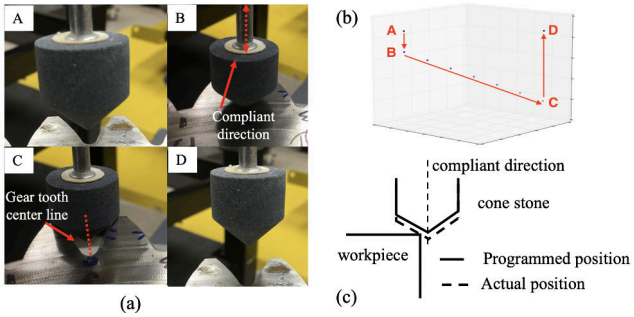


Fig. 4. (a) Chamfering trajectory A: start, B: make contact at gear root, C: finish, D: break contact (b) schematic trajectory illustration (c) compliant mechanism in regulating position uncertainties along the tool axial direction

contact with the gear, then it moves back to the start point. This process is repeated $n$ times and coordinates of the contact points are recorded and the center of the gear is then calculated by formulating a least square problem by using the method proposed by Coope (1993). Then the robot proceeds to gear root identification and chamfering. For gear root identification, assuming there is a designated area where it is safe for the robot end-effector to start the identification process. This can be guaranteed by using fixtures. As is shown in Fig. 3, robot starts with end-effector in the designated area at point $P$ and then moves towards the gear center obtained from previous step. As the cone stone hits the gear at point $P_1$, it begins to slide on the contour of the gear under force control until the cone stone reaches the gear root $P_2$ and contact force is at the preset level. Then $P_2$ is considered as the position of the gear root.

After the gear root identification, the end-effector proceeds to do chamfering and the process is shown in Fig. 4. End-effector moves up to position A so that the spindle can be safely powered on. Then the cone stones moves down to position B to start chamfering. End-effector then traverses along the direction defined by the gear center $O$ and the gear root $P_2$ in Fig. 3 to chamfer both edges until it reaches the out diameter of the gear at position C. End-effector then moves up to break contact with the gear at position D and then gets ready to repeat the same procedure for the next set of gear edges.

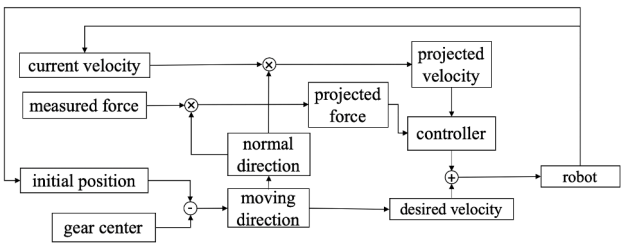


Fig. 5. Force motion control diagram for gear identification

## 4. FORCE AND MOTION CONTROL STRATEGY

This section discusses force and motion control strategy employed in the gear root identification process. In this work, gear root identification based on an impedance

control strategy provides an accurate gear root location. With the identified gear center and gear root location, the motion of the end-effector during chamfering will be following the gear tooth center line as shown in Fig. 4(a). Thus, gear over cut when using cone stone or cutter can be avoided. Additional compliant force control that can compensate for errors along the spindle axis is also discussed.

### *4.1 Force and motion control during identification and chamfering*

Force control in gear root identification process aims to enable the end-effector to slide into the gear root and record the gear root position for trajectory generation while uncertainties exist in the gear position. The control input $\mathbf{u}$ to the robot is a vector of joint velocities. Denote the velocity of the end-effector in robot base frame as $\dot{\mathbf{x}} = [\mathbf{v}, \omega]$ where $\mathbf{v}$ is the translation velocity and $\omega$ is the rotation velocity. During gear root identification, $\omega$ is zero since the axis of the gear is aligned with the $z$-axis of the robot. The translation velocity of the robot end-effector is first expressed in the defined local coordinate frame $x_p$-$y_p$ plane (see Fig. 3) as $\mathbf{v}_{tool} = [v_x, v_y, v_z]$. $v_x$ and $v_y$ are along the $x_p$- and $y_p$- axis, respectively, while $v_x$ is set as a constant value, and $v_y$ is given by the control law. $v_z = 0$ since the motion is within $x_p$-$y_p$ plane. The controller diagram shown in Fig. 5 briefly describes the calculation of the control input $\mathbf{u}$ to the robot. The identified gear center and initial end-effector position decouples the motion control direction and the perpendicular force control direction. The velocity along the force control direction utilizes the projected force, velocity and displacement values. Denote the unit vectors representing the directions of $x_p$- and $y_p$- axis in the robot base frame as $\mathbf{n}$ and $\mathbf{n}_\perp$, which can be calculated by using the positions of the end-effector initial position $\mathbf{X_P}$ (point $P$ in Fig. 3) and the identified gear center $O$. In order for the robot end-effector to exhibit a desired impedance behavior when making contact with the gear, the following relation is desired:

$$a(k+1) = k_f(\mathbf{F_m}(k)\mathbf{n}_\perp - F_d) - k_d v_y(k) - k_p(\mathbf{X}(k) - \mathbf{X_P})\mathbf{n}_\perp \tag{7}$$

$$v_y(k+1) = v_y(k) + a(k+1)T \tag{8}$$

where $a(k+1)$ is the acceleration along the $y_p$-axis at time-step $k+1$, $\mathbf{F_m}(k)$ is the measured force vector at time-step $k$, $F_d$ is the desired force along $y_p$-axis and is set as 0, $v_y(k)$ is the velocity along $y_p$-axis, $\mathbf{X}(k)$ is the end-effector position at time-step $k$, $T$ is the control loop time, $k_f, k_d, k_p$ are the scalar control coefficients. Equation (7) and (8) regulate the impedance behavior of the robot end-effector when making contact with the gear. To transform the calculated velocity $\mathbf{v}_{tool}$ from the local $x_p$-$y_p$ frame into the robot base frame, we utilize the forward kinematics of the robot:

$$T^{tool}_{base} = \prod_{i=1}^{6} T^i_{i-1}(q_i), T^i_{i-1}(q_i) = \begin{bmatrix} R^i_{i-1} & p^i_{i-1} \\ \mathbf{0} & 1 \end{bmatrix} \tag{9}$$

where $T^{tool}_{base}$ is the transformation matrix from robot base frame to tool frame as shown in Fig. 1, $T^i_{i-1}(q_i)$ is the transformation matrix from the $(i-1)$-th joint to the $i$-th joint under joint angle $q_i$, $p^i_{i-1}$ and $R^i_{i-1}$ are the translation vector and rotation matrices between the $(i-1)$th joint and the $i$th joint, respectively, which are determined by the current joint angles and the DH-parameters of the robotic manipulator. Suppose the transformation of the end-effector to the robot base is:

$$T^{tool}_{base} = \begin{bmatrix} R^{tool}_{base} & p^{tool}_{base} \\ \mathbf{0} & 1 \end{bmatrix} \tag{10}$$

Then the desired end-effector velocity in robot base is given by

$$\mathbf{v} = R^{tool}_{base}\mathbf{v}_{tool} \tag{11}$$

Then the control input $\mathbf{u}$ (joint velocity vector) at time-step $k+1$ is calculated by using current Jacobian $\mathbf{J}$:

$$\mathbf{u}(k+1) = \mathbf{J}(\mathbf{q}(k))^{-1}\dot{\mathbf{x}}(k+1) \tag{12}$$

Once the gear root is identified, we can design the trajectory of travel between the two gear teeth for the cone stone to perform the chamfering operation, which is illustrated in Fig. 4. The end-effector starts at position A in Fig. 4(a) at which time the spindle is powered. Then the end-effector moves to position B to initiate gear chamfering. The chamfering process takes place along B and C and cone stone breaks contact with the gear from C to D in order to move to the next gear tooth. During chamfering (B to C), force along the spindle axis is regulated by a compliant device so that the contact between the cone stone and the gear is guaranteed and provide force for the chamfering of the two edges of the adjacent gears. The effectiveness of this proposed strategy can be seen through the experimental results provided in Section 5.

Free motion phases are pure velocity based position control of the robot. Denote the target position as $T^d_{base}$, then the transformation matrix from current tool position to the desired position can be calculated by:

$$T^{tool}_{base}T^d_{tool} = T^d_{base}, \quad T^d_{tool} = (T^{tool}_{base})^{-1}T^d_{base} \tag{13}$$

The matrix $T^d_{tool}$ is the transformation that is needed for the robot to move the end-effector to the desired configuration, and can be considered as the error matrix. The rotation part of the error matrix $R^d_{tool}$ is transformed into an axis-angle representation form for calculation of joint velocities for the next time step. The axis-angle representation of the rotation error is obtained in the following manner based on the work of Altmann (2005):

$$\theta = \arccos\left(\frac{Tr(R^d_{tool}) - 1}{2}\right) \tag{14}$$

$$\mathbf{s} = \frac{1}{2\sin(\theta)} \begin{bmatrix} R^d_{tool}(3,2) - R^d_{tool}(2,3) \\ R^d_{tool}(1,3) - R^d_{tool}(3,1) \\ R^d_{tool}(2,1) - R^d_{tool}(1,2) \end{bmatrix} \tag{15}$$

where $\theta(\theta \neq 0)$ is the rotation angle around the axis $\mathbf{s}$, $Tr(\cdot)$ calculates the trace of the rotation matrix. A proportional controller with coefficient $k_\omega$ is employed to generate rotational velocity $\omega = k_\omega\theta\mathbf{s}$, and the translation velocity input $\mathbf{v}$ is also obtained as a proportional controller on the position error $p^d_{tool}$ to maneuver the end-effector to the desired position.

### *4.2 Compliant device*

Considering the shape of the cone stone, the displacement of the end-effector along the spindle axis should be equal to the distance between the start and final contact points on the cone stone in order for the cone stone to maintain contact with the gear during the chamfering of the entire

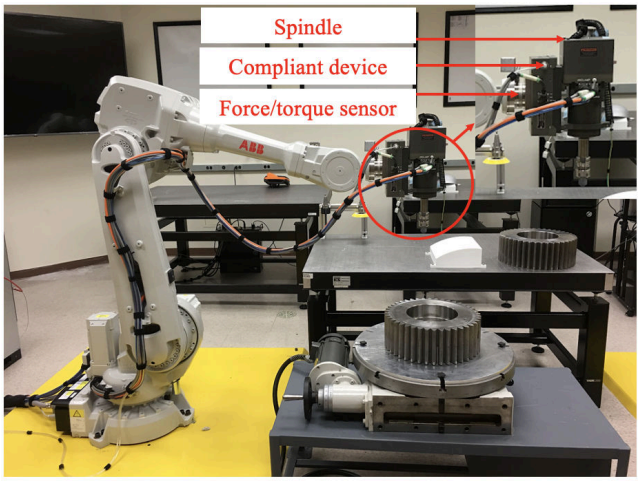


Fig. 6. Experimental setup

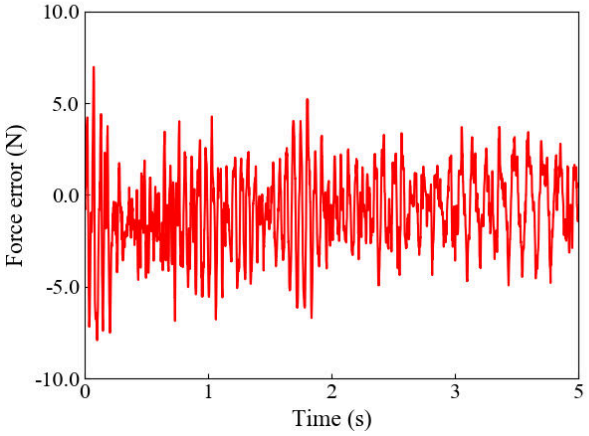


Fig. 7. Force error during examination

edge. We utilize a compliant device that can maintain the force along the spindle axis. The benefits of using a compliant device are twofold. First, it helps in maintaining the contact between the chamfering cone stone and the two gear edges even in the presence of possible position uncertainties. Fig. 4(c) shows the movement of the compliant device when there is an error between the programmed position and the actual workpiece position along $z$ axis. The position of the end-effector can be adjusted by the compliant device in order to maintain contact with the gear edges under this uncertainty. Second, the compliant force acts as the force required for material removal for chamfering. By changing the compliant force, force exerted on the gear that comes from chamfering cone stone will change accordingly.

## 5. EXPERIMENTS AND RESULTS

### *5.1 Hardware and software setup*

The experimental setup is shown in Fig. 6. It consists of a six DOF robotic manipulator ABB IRB-4600, a six-axis force/torque sensor Omega 85 from ATI, an eletric spindle, and a compliant device AFD 310 from Pushcorp. The compliant device and the spindle are mounted such that the compliant force is regulated along the spindle axis. The workpiece is a large gear with diameter 14" and contains 42 gear teeth in total. When the gear is cut, it has sharp edges on the gear tooth which need to be chamfered. A chamfering cone stone with a pointed tip is used. Real-time control is implemented using Robot Operating System (ROS), and the External Guided Motion (EGM) module from ABB along with the open source ROS package 'abb_libegm' are used to access robot joint velocities, and receive velocity commands from PC.

### *5.2 Effectiveness of force/motion control*

To quantify the effectiveness of the force/motion control, the robot is commanded to move along the chamfering trajectory in Fig. 4(b) after the gear root is identified, but without powering the spindle. The force error perpendicular to the gear center line is measured, see Fig. 7. The reason for not powering the spindle during this evaluation is that if the generated trajectory is correct, then the cone stone will follow the current gear tooth center line, then the force error projected on the direction that is perpendicular to the gear tooth center line will be zero. Then, force control perpendicular the gear center line is not necessary during chamfering. As shown in Fig. 7, the force error in the direction that is perpendicular to current gear tooth center line has a mean value that is close to zero. The oscillations in the force signal can be explained by the fact that the cone stone does not have a smooth surface due to the abrasive on it, so the contact force tends to change as the cone stone is moving on the gear. The small force error normal to the gear center line is indicative of the cone stone is traveling along the actual gear tooth center line.

### *5.3 Chamfering*

The chamfering process is illustrated in Fig. 8(a) and the chamfered gear teeth are shown in Fig. 8(b). Compliant force is set at 13.35 N (3.0 lbs) during experiments. During experiments, the process of gear root identification and chamfering are combined together. Chamfer cone stone first slides into gear root to identify the position with the spindle powered off, then the spindle moves up, powered on, and then moves down to make contact with the gear. The cone stone then travels along the center line of the gear root while chamfering both edges. For the experiment, the trajectory for each pair of gear teeth is determined individually to reduce error accumulation, i.e. all gear roots are identified. The possibility of identifying certain amount of gear roots to reduce identification time will be explored in future work. Chamfers quality shown in Fig. 8 are uniform indicating the effectiveness of this method.

### *5.4 Compliant force, spindle speed and material removal*

The material removal force for the chamfering operation is due to the maintenance of the compliant force along spindle axis by the compliant device. Material removal, i.e., chamfer width, is related to the compliant force as well as the rotation speed of the spindle. Experiments were conducted to evaluate the effect of the compliant force on chamfer width at a fixed spindle speed of 5,250 revolutions

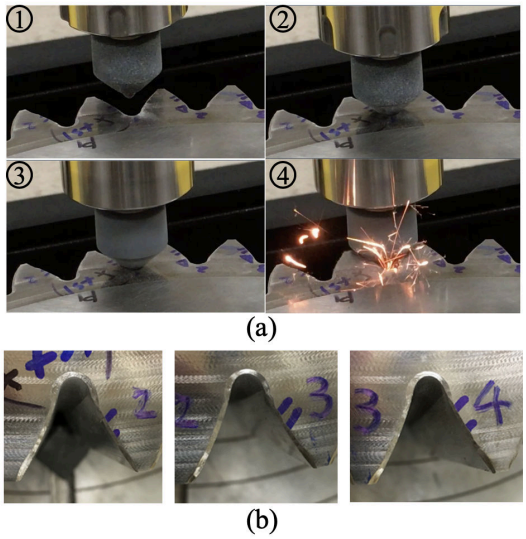


Fig. 8. Chamfering process and obtained chamfers: (a) step 1, 2 correspond to the identification process in Fig. 3, step 3, 4 correspond to the chamfering process in Fig. 4; (b) obtained chamfers

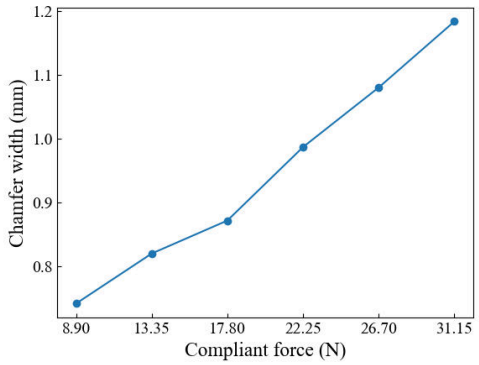


Fig. 9. Relation between compliant force and chamfer width

per minute (RPM). The results for different values of the compliant force (used lbs in experiments) are provided in Fig. 9. The compliant force can be selected to generate desired chamfer width.

## 6. CONCLUSION

Registration errors associated with placement of the workpiece in the workspace of the robot is a significant impediment to automation of robotic manufacturing operations such as deburring, chamfering, and grinding. Because of this difficulty, most cast and cut parts are finished by human operators using hand-held tools. For some simpler geometries, CNC machine can be used for contour following approach, especially for small gears; this method relies heavily on accurate registration of the workpiece in the work cell which can be time-consuming and costly. In this paper, we proposed a novel force/motion control method to identify and compensate for registration errors for robotic chamfering operations, especially for complex contoured parts such as gears. The identification process proposed in this work provides the coordinates of the gear center and gear roots to generate a novel chamfering trajectory that can be employed to chamfer two edges of adjacent gear teeth simultaneously. We have proposed a force/motion control strategy to facilitate gear root identification and edge chamfering. Results from a number of chamfering experiments in terms of chamfer quality and chamfer width corroborate the effectiveness of the proposed method. Further, the proposed method reduces setup time and registration time of the workpiece in the robotic work cell.

## ACKNOWLEDGEMENTS

The authors want to thank Cara Mazzarini for her help and guidance throughout the ARM funded project.

## REFERENCES

Altmann, S.L. (2005). *Rotations, quaternions, and double groups*. Courier Corporation.

Asakawa, N., Toda, K., and Takeuchi, Y. (2000). Automation of chamfering by an industrial robot; for the case of hole on a free curved surface. *IFAC Proceedings Volumes*, 33(17), 1215 – 1220.

Coope, I.D. (1993). Circle fitting by linear and nonlinear least squares. *Journal of Optimization Theory and Applications*, 76(2), 381–388.

Kashiwagi, K., Ono, K., Izumi, E., Kurenuma, T., and Yamada, K. (1990). Force controlled robot for grinding. In *EEE International Workshop on Intelligent Robots and Systems, Towards a New Frontier of Applications*, 1001–1006 vol.2.

Kuss, A., Drust, M., and Verl, A. (2016). Detection of workpiece shape deviations for tool path adaptation in robotic deburring systems. *Procedia CIRP*, 57, 545 – 550.

Pagilla, P.R. and Yu, B. (2001a). Adaptive control of robotic surface finishing processes. In *Proceedings of the 2001 American Control Conference.*, volume 1, 630–635 vol.1.

Pagilla, P.R. and Yu, B. (2001b). Robotic surface finishing processes: Modeling, control, and experiments. *Journal of Dynamic Systems Measurement and Control-transactions*, 123, 93–102.

Pagilla, P.R. and Yu, B. (2002). Mechatronic design and control of a robot system interacting with an external environment. *Mechatronics*, 12(6), 791 – 811.

Song, H.C. and Song, J.B. (2013). Precision robotic deburring based on force control for arbitrarily shaped workpiece using cad model matching. *International Journal of Precision Engineering and Manufacturing*, 14(1), 85–91.

Wen, Y., Hu, J., and Pagilla, P.R. (2019). A novel robotic system for finishing of freeform surfaces. In *2019 International Conference on Robotics and Automation (ICRA)*, 5571–5577.

Zhang, H., Chen, H., Xi, N., Zhang, G., and He, J. (2006). On-line path generation for robotic deburring of cast aluminum wheels. In *2006 IEEE/RSJ International Conference on Intelligent Robots and Systems*, 2400–2405.

Ziliani, G., Visioli, A., and Legnani, G. (2007). A mechatronic approach for robotic deburring. *Mechatronics*, 17(8), 431 – 441.